Eur. Phys. J. B **41**, 313–318 (2004)
DOI: 10.1140/epjb/e2004-00323-6

**THE EUROPEAN PHYSICAL JOURNAL B**

# Microwave properties of $Ba_{0.6}K_{0.4}BiO_3$ crystals

S. Fricano[1], M. Bonura[1], A. Agliolo Gallitto[1,a], M. Li Vigni[1], L.A. Klinkova[2], and N.V. Barkovskii[2]

[1] INFM and Dipartimento di Scienze Fisiche e Astronomiche, Università di Palermo, Via Archirafi 36, 90123 Palermo, Italy
[2] Institute of Solid State Physics, Chernogolovka, Moscow District 142432, Russia

Received 6 May 2004 / Received in final form 29 July 2004
Published online 21 October 2004 – 

**Abstract.** We report on field-induced variations of the microwave surface resistance at 9.6 GHz of $Ba_{0.6}K_{0.4}BiO_3$ crystals. Energy losses have been investigated as a function of the static magnetic field in the range of temperatures 4.2 K $\div$ $T_c$. By analyzing the experimental results in the framework of the Coffey and Clem model we determine the temperature dependence of the first-penetration field, upper critical field and depinning frequency. The results show that the pinning energy of this bismuthate superconductor is weaker than those of cuprates.

**PACS.** 74.25.Ha Magnetic properties – 74.25.Nf Response to electromagnetic fields (nuclear magnetic resonance, surface impedance, etc.) – 74.25.Op Mixed states, critical fields, and surface sheaths

## 1 Introduction

The bismuthate superconductor $Ba_{0.6}K_{0.4}BiO_3$ (BKBO) is often classified as a high-temperature superconductor because of the relatively high critical temperature, $T_c \simeq 30$ K well above that of conventional superconductors. The interest in the study of the BKBO compound is due to the fact that, although it does not contain copper, some characteristics are similar to those of cuprate superconductors: it is an oxide with perovskite structure, low charge-carrier density and superconductivity near a metal-insulator transition [1–3]. Despite such similarities, some marked differences can be highlighted: bismuthates are nonmagnetic, and they have three-dimensional structures rather than layered two-dimensional ones characteristic of cuprates [4]. Though several properties of BKBO have been explained in the framework of the BCS theory [5,6], with a single type of carrier pairing, anomalies such as, e.g., the upward curvature at temperatures near $T_c$ of the upper critical field, cannot be explained in the weak-coupling limit [7–11]. A complication in interpreting the experimental results is related to the intrinsic difficulty of producing BKBO crystals with a highly uniform K-ion content. Indeed, the presence of micro-domains with different potassium concentration, which could strongly affect several physical properties, seems to be an intrinsic feature of the available BKBO samples.

The magnetic properties of BKBO have been investigated by different techniques such as magnetic susceptibility, specific heat and thermal conductivity measurements [1,9,12]. The results have highlighted very small values of the pinning energy, consistent with those measured in other bismuthate superconductors [13]. This small pinning energy is responsible for the enhanced dissipation and the low critical current observed in the bismuthate superconductors. Usually, the pinning characteristics are extracted from the field dependence of the critical current; however, since the critical current of high-$T_c$ superconductors at low temperatures is too large to be measured by direct-contact method, the study of the electromagnetic (*em*) response of superconductors in the mixed state is a more convenient method. Measurements of high-frequency *em* response are particularly suitable to investigate vortex dynamics because they probe the vortex response at very low currents, when the vortices undergo reversible oscillations [14]. The most commonly method to study the high-frequency *em* response consists in measuring the microwave (*mw*) surface impedance, $Z_s = R_s - iX_s$ [14,15]. The real component, $R_s$, is proportional to the energy losses while the imaginary component, $X_s$, is related to the field penetration depth. The different vortex states, in the different regions of the $H$-$T$ phase diagram, determine the temperature and field dependencies of $Z_s$; so, measurements of $Z_s(H,T)$ may provide important information on the fluxon dynamics in the different regimes of motion [14,16–18].

In this paper, we report experimental results of field-induced variations of $R_s$ in a single crystal of BKBO. The experimental results allow measuring the values of the magnetic field at which fluxons start to penetrate the sample and the temperature dependence of the upper critical field. The experimental curves of $R_s(H,T)$ are well

[a] e-mail: agliolo@fisica.unipa.it

accounted for in the framework of the Coffey and Clem model [17] in the whole range of temperatures investigated ($4.2\ \mathrm{K} \div T_c$). By fitting the experimental data, using this model, we have deduced the temperature dependence of the depinning frequency. Near $T_c$, the *mw* current induces fluxons moving in the flux-flow regime and the depinning frequency is almost zero; it remains roughly zero for $\approx 8$ K below $T_c$; on further decreasing the temperature, the value of the depinning frequency increases up to $\sim$20 GHz at $T = 4.2$ K. This value confirms that even at low temperatures the pinning energy is small; so that, the motion of weakly-pinned fluxons, induced by the *mw* current, gives rise to relatively large energy losses.

## 2 Experimental and sample

The field-induced variations of $R_s$ have been studied in a single crystal of BKBO of nearly cubic shape, with about 1 mm edge; it undergoes a superconducting transition at $T_c \approx 32$ K, of width $\approx 2.5$ K. The sample has been synthesized at the Institute of Solid State Physics of Russian Academy of Science. It has been produced by electrolysis of KOH-$Ba(OH)_2$-$Bi_2O_3$ melt, under conditions of stationary mass transfer [19]. The $Ba_{1-x}K_xBiO_3$ crystals produced with this method have a potassium concentration near to the optimal value, $x \approx 0.4$. However, they exhibit a wide superconducting transition and a considerable residual *mw* surface resistance at low temperatures. These features can be ascribed to an inhomogeneous distribution of K ions in the crystals [20].

The *mw* surface resistance has been measured using the cavity perturbation technique [15]. The copper cavity, of cylindrical shape with golden-plated walls, is tuned in the $TE_{011}$ mode resonating at 9.6 GHz ($Q \approx 40,000$ at $T = 4.2$ K). It is placed between the poles of an electromagnet, which generates static magnetic fields, $H_0$, up to $\approx 10$ kOe. Two additional coils, independently fed, allow compensating the residual field and working at low magnetic fields. The sample is put in the center of the cavity by a sapphire rod, in the region of maximum *mw* magnetic field. The sample and field geometry is shown in Figure 1a; in this geometry the *mw* current induces a tilt motion of all the fluxons present in the sample, as shown in Figure 1b. The $Q$-factor of the cavity is measured by means of an *hp*-8719D Network Analyzer. The surface resistance of the sample is proportional to $(1/Q_L - 1/Q_U)$, where $Q_U$ is the $Q$-factor of the empty cavity and $Q_L$ is that of the loaded cavity. In order to disregard the geometric factor of the sample, it is convenient to normalize the deduced values of $R_s$ to the value of the surface resistance at a fixed temperature in the normal state, $R_n$. In particular, we have normalized all the $R_s$ values here reported to the value of $R_n$ at $T = 32$ K and $H_0 = 0$. Measurements have been performed as a function of the temperature and the static magnetic field.

Figure 2 shows the temperature dependence of the normalized surface resistance, at different values of the static field. The results have been obtained according to the following procedure: the sample was zero-field cooled (ZFC)

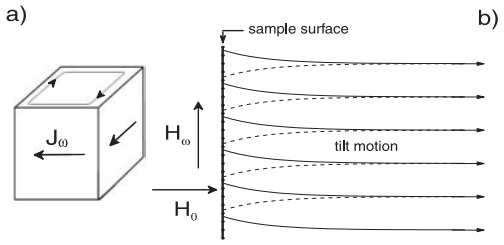


**Fig. 1.** a) Sample and field geometry. b) Fluxon motion induced by the *mw* current; the arrows indicate the flux lines.

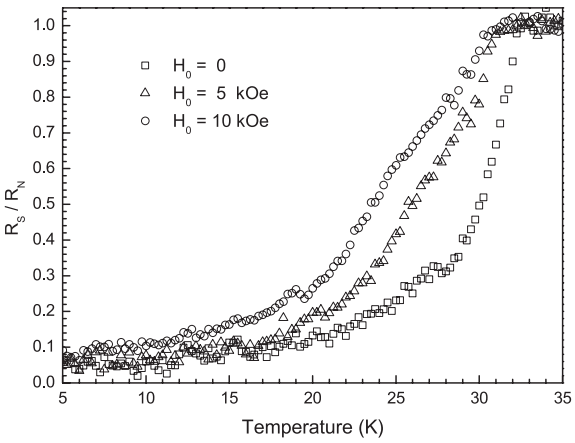


**Fig. 2.** Normalized values of the *mw* surface resistance as a function of the temperature, for different values of $H_0$.

down to 4.2 K, then $H_0$ was set at a given value, which was kept constant during the time in which the measurements in the temperature range $4.2 \div 32$ K have been performed. As expected, on increasing $H_0$, the $R_s(T)$ curve broadens and shifts toward lower temperatures. Measuring the temperature and field at which $R_s/R_n = 1$, we have estimated $dH_{c2}(T)/dT|_{T_c} \sim 5$ kOe/K, in agreement with the results reported in the literature [7].

$R_s$ has also been investigated as a function of the magnetic field, in the range $0 \leq H_0 \leq 10$ kOe, at fixed values of temperature. Each measurement has been performed, in the ZFC sample, sweeping the external field up to 10 kOe and, successively, decreasing it down to zero, at constant temperature. Figure 3 shows $R_s/R_n$ as a function of $H_0$ at $T = 4.2$ K. Open and solid symbols refer to results obtained on increasing and decreasing $H_0$, respectively; no magnetic hysteresis has been observed. In order to better highlight the low-field dependence of $R_s/R_n$, in the inset we report the data in a semi-log plot. As one can see, the curve is field independent in the range $0 \div H_p$, showing that, in this range, the external magnetic field does not induce variations of the surface resistance. Since the sample was ZFC, $H_p$ should mark the first-penetration field.

Figure 4 shows the normalized values of the surface resistance as a function of the static magnetic field, at different values of the temperature in the range $10 \div 30$ K; symbols show the experimental data, lines are the best-fit curves of data obtained with the procedure described in

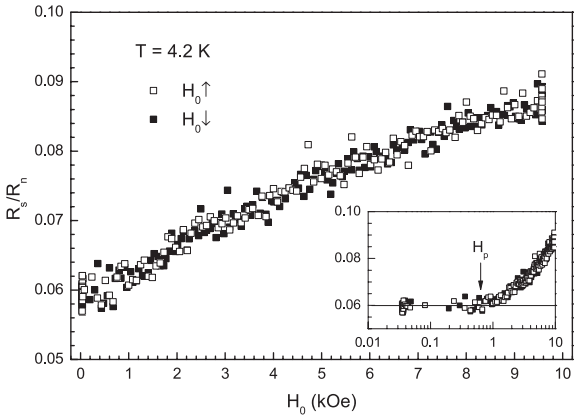


**Fig. 3.** Normalized values of $R_s$ as a function of the static magnetic field at $T = 4.2$ K. Open and solid symbols refer to results obtained on increasing and decreasing field, respectively. The arrow in the inset indicates the first-penetration field, $H_p$.

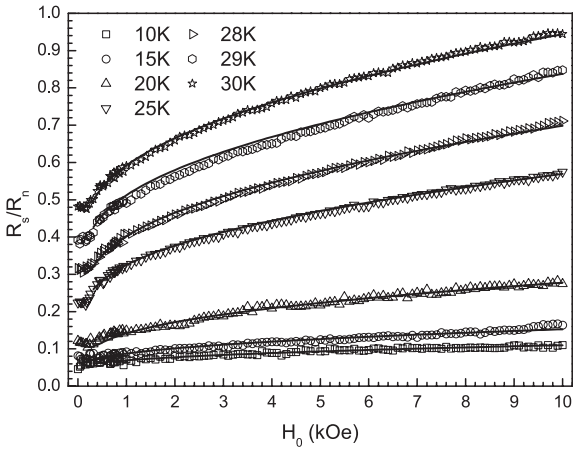


**Fig. 4.** Normalized values of $R_s$ as a function of the static magnetic field, for different values of temperature. The lines are the best-fit curves, obtained as described in Section 3.

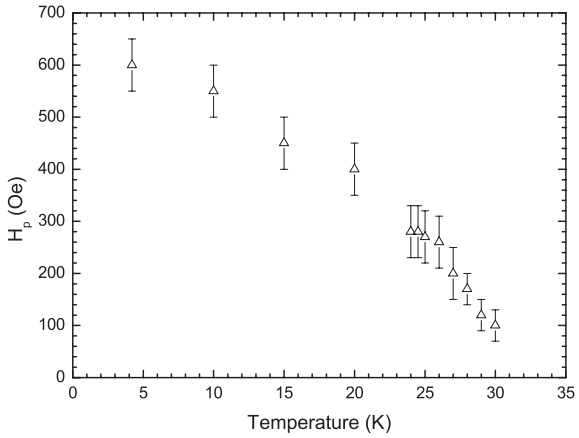


**Fig. 5.** Temperature dependence of the first-penetration field, $H_p$. The symbols show the $H_p$ values deduced from the $R_s(H,T)$ curves, as the $H_0$ values at which $R_s$ starts increasing.

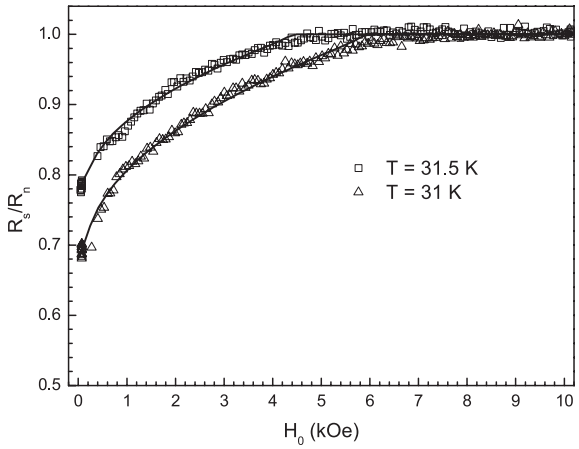


**Fig. 6.** Normalized values of $R_s$ as a function of $H_0$, for two values of temperature close to $T_c$. The lines are the best-fit curves, obtained as described in Section 3.

the next section. As one can see, on increasing the temperature the field-induced variations of $R_s$ increase. By analyzing the experimental data of Figures 3 and 4 obtained at low applied fields, we have deduced the temperature dependence of the first-penetration field, which is shown in Figure 5. As one can see, on decreasing the temperature $H_p$ increases monotonically even at low temperatures; this behavior has already been reported by Hall et al. [10]. The value of $H_p(0)$ results slightly larger than the $H_{c1}(0)$ values reported in the literature for BKBO crystals [1,10], suggesting that weak surface-barrier effects are present in our sample.

In Figure 6 we report the normalized values of the surface resistance as a function of the static magnetic field at temperatures near $T_c$. The symbols show the experimental data, the lines have been obtained by fitting the data with the procedure described in the next section. At temperatures close to $T_c$, the sample goes into the normal state at $H_0$ values that our experimental apparatus can easily supply. At a fixed temperature, measuring the value of $H_0$ at which $R_s$ reaches the normal-state value we have determined $H_{c2}(T)$; the deduced values are consistent with those obtained from the $R_s$-vs.-$T$ curves and those reported in the literature for BKBO crystals [7].

## 3 Discussion

Microwave losses induced by the static magnetic field in superconductors in the mixed state are mainly due to the motion of fluxons and, at temperatures near $T_c$, to the very presence of vortices, which bring along normal fluid in their core [17,21]. For ZFC samples, on increasing the static magnetic field, the surface resistance begins to increase when $H_0$ reaches the value at which fluxons start penetrating the sample. So, in our results the value of the field indicated with $H_p$ (see inset in Fig. 3) marks the first-penetration field. From Figure 5, one can

see that the values of $H_p$ obtained at the lowest temperature investigated are slightly larger than the values of $H_{c1}(0)$ reported in the literature for BKBO crystals [1], suggesting that in our sample weak surface-barrier effects are present. However, since at temperatures close to $T_c$ the surface-barrier effects are negligible, in this range of temperatures, $H_p$ should coincide with $H_{c1}$. As one can see from Figure 5, the $H_p(T)$ curve does not exhibit upward curvature near $T_c$, in contrast to what occurs in the $H_{c2}(T)$ curve of BKBO [7–9,11]. This is a peculiar property of BKBO; indeed, though in conventional superconductors $H_{c1}$ and $H_{c2}$ near $T_c$ have the same temperature dependence, in BKBO they show different behavior. Studies reported in the literature on the origin of this property have suggested that the upward curvature of $H_{c2}(T)$ is due to intrinsic disorder in the crystal structure of BKBO [9]. The reason for which this does not influence $H_{c1}(T)$, leading to the absence of the upward curvature, is still unclear.

The field-induced variations of $R_s$ in the mixed state have been studied by different authors [14,17,18]. Coffey and Clem (CC) have developed a comprehensive theory for the *em* response of type-II superconductors in the mixed state, in the framework of the two-fluid model [17]. The theory applies for $H_0 > 2H_{c1}$, when the induction field inside the sample can be supposed as generated by an uniform density of fluxons; in this case $H_0 \approx B_0 = n\phi_0$, where $\phi_0$ is the flux quantum and $n$ is the vortex density. We will show that our results can be well accounted for by the CC model taking into consideration that in different temperature ranges the *mw* current induces fluxons moving in different regimes.

In the London local limit, the surface impedance is proportional to the complex penetration depth of the *em* field, $\widetilde{\lambda}$. In particular

$$R_s = -\frac{4\pi\omega}{c^2}\Im(\widetilde{\lambda}). \tag{1}$$

In the CC model $\widetilde{\lambda}$ is calculated by taking into account the effects of the fluxon motion and the very presence of vortices. In the linear approximation, $H(\omega) \ll H_0$, the following expression for $\widetilde{\lambda}$ has been obtained [17]:

$$\widetilde{\lambda}^2 = \frac{\lambda^2 + \widetilde{\delta}_v^2}{1 - 2i\lambda^2/\delta^2}, \tag{2}$$

where $\widetilde{\delta}_v$ is the effective complex skin depth arising from vortex motion; $\lambda$ and $\delta$, the London penetration depth and the normal-fluid skin depth, are given by

$$\lambda = \frac{\lambda_0}{\sqrt{(1-w)(1-B_0/H_{c2})}}, \tag{3}$$

$$\delta = \frac{\delta_0}{\sqrt{1-(1-w)(1-B_0/H_{c2})}}, \tag{4}$$

here $\lambda_0$ is the London penetration depth at $T = 0$; $\delta_0$ is the normal-fluid skin depth at $T = T_c$; $w$ is the fraction of normal electrons at $H_0 = 0$, in the Gorter and Casimir two-fluid model $w = (T/T_c)^4$.

The penetration depth $\widetilde{\delta}_v$ can be written in terms of the two characteristic lengths, $\delta_f$ and $\lambda_c$, arising from the contributions of the viscous and the restoring-pinning forces, respectively:

$$\frac{1}{\widetilde{\delta}_v^2} = \frac{1}{\lambda_c^2} - \frac{2i}{\delta_f^2}, \tag{5}$$

where

$$\lambda_c^2 = \frac{B_0\phi_0}{4\pi k_p}, \tag{6}$$

$$\delta_f^2 = \frac{B_0\phi_0}{2\pi\omega\eta}, \tag{7}$$

with $k_p$ the restoring-force coefficient and $\eta$ the viscous-drag coefficient. In *s*-wave superconductors, such as BKBO [22,23], the viscous-drag coefficient is given by the Bardeen-Stephen expression [24]

$$\eta = \frac{\phi_0 H_{c2}}{\rho_n c^2}, \tag{8}$$

where $\rho_n$ is the normal-state resistivity.

The effectiveness of the two terms in equation (5) depends on the ratio $\omega_c = k_p/\eta$, which defines the depinning frequency. In terms of $\omega_c$, equation (5) can be written as

$$\frac{1}{\widetilde{\delta}_v^2} = \frac{1}{4\delta_f^2}\left(\frac{\omega_c}{\omega} - \frac{i}{2}\right). \tag{9}$$

When the frequency of the *em* wave, $\omega$, is much larger than $\omega_c$ the contribution of the viscous-drag force predominates and the induced *em* current makes fluxons move in the flux-flow regime. On the contrary, for $\omega \ll \omega_c$ the motion of fluxons is ruled by the restoring-pinning force.

It is worth noting that the above-mentioned expressions have been obtained by supposing that the *em* current induces compressional waves of the fluxon-line lattice within the field penetration depth; as a consequence, $B_0$ is the induction field within $\widetilde{\lambda}$. In the field geometry of our experimental apparatus, the *mw* current induces a *tilt* motion of all the fluxons present in the sample. On the other hand, Brandt [18] has shown that the *compressional* and *tilt* motion can be described by the same formalism, and the same complex penetration depth results since the moduli for long-wavelength compression and tilt are approximately equal. So, we can consider valid the expressions obtained in the CC model provided that $B_0$ be the induction field averaged over the whole sample.

Equations (1–9) allow calculating the field-induced variations of the surface resistance, at fixed values of the temperature. However, they cannot account for the residual surface resistance, measured at zero dc field, which is mainly related to the sample inhomogeneity. In order to compare the expected and experimental results, at fixed temperature values, we have calculated the field-induced variations of $R_s/R_n$ normalized to the maximal value:

$$\frac{[R_s(H,T) - R_s(0,T)]/R_n}{1 - R_s(0,T)/R_n} = \frac{2\Im[\widetilde{\lambda}(H,T) - \widetilde{\lambda}(0,T)]/\delta_0}{1 - 2\Im(\widetilde{\lambda}(0,T))/\delta_0}, \tag{10}$$

where the left-side term can be determined from the experimental data and the right-side term is the expected one, $\delta_0/2$ corresponds to the value of $\Im(\widetilde{\lambda})$ in the normal state.

By considering the values of the characteristic parameters of BKBO crystals, it can be shown that, except at temperatures very close to $T_c$, $\Im[\widetilde{\lambda}(0,T)] \ll \delta_0/2$. Therefore, from equation (10) it results:

$$\frac{R_s(H,T)}{R_n} \simeq \frac{R_s(0,T)}{R_n} + \left[1 - \frac{R_s(0,T)}{R_n}\right] \frac{2\Im[\widetilde{\lambda}(H,T) - \widetilde{\lambda}(0,T)]}{\delta_0}. \quad (11)$$

Equation (11) has been used to fit the experimental data[1]. It is worth remarking that only the experimental results obtained for $H_0 > H_p$ have been fitted.

At temperatures near $T_c$ the induced $mw$ current makes fluxons move in the flux-flow regime, so we can assume $\omega \gg \omega_c \approx 0$. In this case, $\delta_v^2 \approx i\delta_f^2/2$ and, in order to perform a comparison between the experimental and the expected $R_s(H,T)$ curves, besides $R_s(0,T)/R_n$, only two parameters are necessary: the ratio $\lambda_0/\delta_0$ and $H_{c2}(T)$. Since, at temperatures near $T_c$, the $H_{c2}(T)$ values can be directly deduced from the $R_s(H,T)$ curves, the only free parameter necessary for fitting the experimental data, obtained near $T_c$, is $\lambda_0/\delta_0$. The lines in Figure 6 have been obtained by equation (11) using for $H_{c2}(T)$ and $R_s(0,T)/R_n$ the values deduced from the experimental results, letting them vary within the experimental uncertainty, and taking $\lambda_0/\delta_0$ as free parameter. The best-fit curves of Figure 6 have been obtained with $\lambda_0/\delta_0 = 0.04$; however, we have found that the expected results are little sensitive to variations of $\lambda_0/\delta_0$ as long as it takes on values of the order of $10^{-2}$. It is easy to see that $\lambda_0/\delta_0 = \sqrt{\omega\tau/2}$, where $\tau$ is the scattering time of the normal electrons; so the corresponding value of $\tau$ is of the order of $10^{-14}$ s. This value agrees with the ones reported in the literature for BKBO and is smaller than that reported for cuprate superconductors [15,20,25].

For $T \leq 30$ K, the $H_{c2}(T)$ values cannot be directly deduced from the experimental $R_s(H,T)$ results. So, by keeping for $\lambda_0/\delta_0$ the same value obtained at temperatures near $T_c$, the parameters necessary to fit the experimental data are $\omega_c$ and $H_{c2}(T)$. Since $H_{c2}(T)$ of our sample at temperatures near $T_c$ agrees quite well with the values reported in the literature for BKBO crystals [7], we have assumed that even at lower temperatures the values of $H_{c2}(T)$ of our sample are consistent with those reported in the literature. The lines reported in Figure 4 have been obtained by equation (11) taking $\lambda_0/\delta_0 = 0.04$, $\omega_c$ as free parameter and letting $H_{c2}(T)$ vary compatibly with the values reported in the literature for BKBO crystals. As one can see, the expected results describe quite well the experimental data in the whole range of temperatures investigated. In Figure 7 we report the temperature dependence of the upper critical field as deduced by the fitting procedure.

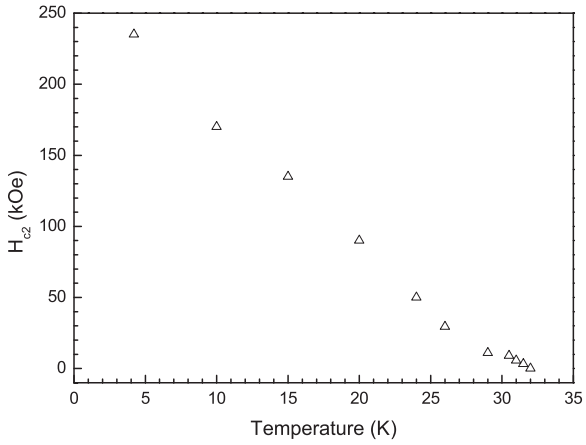


**Fig. 7.** Values of the upper critical field determined as best-fit parameters of the experimental data, using the procedure described in the text.

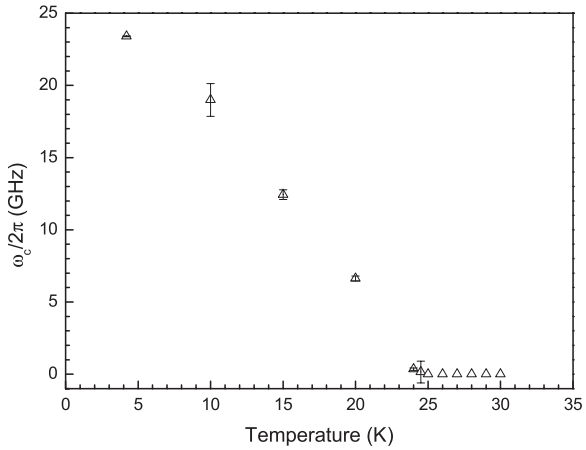


**Fig. 8.** Depinning frequency as a function of the temperature, determined as described in the text.

The values of $\omega_c(T)$ which best fit our experimental data are plotted in Figure 8. In the range of temperatures 25 K $< T < T_c$, $\omega_c$ is zero, within the experimental accuracy; it means that for $T > 25$ K the condition $\omega \gg \omega_c$ is verified and the fluxons, under the action of the $mw$ current, move in the flux-flow regime. On decreasing the temperature the depinning frequency increases, reaching the value $\omega_c/2\pi \simeq 23.4$ GHz at $T = 4.2$ K; this value is lower than the ones reported in the literature for cuprate superconductors. From this value of $\omega_c$, using equation (8) we obtain $k_p \simeq 3.5 \times 10^3$ N/m$^2$ at $T = 4.2$ K. As a consequence of the small value of $\omega_c$, we obtained a pinning constant smaller than that of cuprate superconductors, in agreement with what reported in the literature for

[1] The approximation used to get equation (11) has been verified by numerical calculations using the values of the characteristic parameters of BKBO ($H_{c1}, H_{c2}, T_c, \lambda_0$ and $\delta_0$); it gives rise to corrections much smaller than the experimental uncertainty up to a few tenths of K below $T_c$.

BKBO [1]. As it is well known, the pinning constant is determined by the interaction between vortices and pinning centers as well as by the vortex elasticity. Whereas the effects of the pinning centers may depend on the investigated sample, the vortex elasticity is an intrinsic property of the compound and, usually, its contribution is weaker than the previous one. The value we found for $k_p$ confirms that, even at low temperatures, the pinning energy in BKBO is smaller than in cuprate superconductors, suggesting that the density of pinning centers and the vortex elasticity are too small to prevent *mw* absorption.

## 4 Conclusions

In this paper we have reported a detailed study of the field-induced variations of the *mw* surface resistance in a crystal of BKBO. The *mw* energy losses have been investigated as a function of the temperature and the static magnetic field. We have shown that the experimental results can be well accounted for in the framework of the Coffey and Clem model provided that different regimes of fluxon motion are hypothesized in different ranges of temperature. We have determined the temperature dependence of the first-penetration field and the upper critical field. The values of $H_p(T)$ have been directly deduced from the experimental data in the whole range of temperatures investigated. The temperature dependence of the upper critical field has been obtained determining $H_{c2}(T)$ as fitting parameter. Furthermore, by fitting the experimental data we have determined the temperature dependence of the depinning frequency in the whole range of temperatures investigated. For $\sim$8 K below $T_c$, we have found $\omega_c/\omega \ll 1$, that means that the *mw* current induces fluxons moving in the flux-flow regime. On further reducing the temperature, the depinning frequency increases, reaching the value $\omega_c/2\pi \simeq 23.4$ GHz at $T = 4.2$ K. This finding confirms that in this superconductor the pinning effects are weaker than in the cuprate superconductors and accounts for the enhanced energy losses and the low value of the critical current, reported in the literature for bismuthate superconductors.

The authors are very glad to thank E.H. Brandt, G.E. Tsydynzhapov, I. Ciccarello and M. Guccione for critical reading of the manuscript and helpful suggestions; G. Lapis and G. Napoli for technical assistance. Work partially supported by the University of Palermo (grant Coll. Int. Li Vigni).

## References

1. S.N. Barilo, S.V. Shiryaev, V.I. Gatalskaya, J.W. Lynn, M. Baran, H. Szymczak, R. Szymczak, D. Dew-Hughes, Phys. Rev. B **58**, 12355 (1998)
2. J.H. Lee, K. Char, Y.W. Park, L.Z. Zhao, D.B. Zhu, G.C. McIntosh, A.B. Kaiser, Phys. Rev. B **61**, 14815 (2000)
3. D.G. Hinks, B. Dabrowski, J.D. Jorgensen, A.W. Mitchell, D.R. Richards, S. Pei, D. Shi, Nature **333**, 836 (1988)
4. L.A. Klinkova, M. Uchida, Y. Matsui, V.I. Nikolaichik, N.V. Barkovskii, Phys. Rev. B **67**, 140501(R) (2003)
5. H. Sato, H. Takagi, S. Huchida, Physica C **169**, 391 (1990)
6. D.G. Hinks, D.R. Richards, B. Dabrowski, D.T. Marx, A.W. Mitchell, Nature **335**, 419 (1988)
7. M. Affronte, J. Marcus, C. Escribe-Filippini, A. Sulpice, H. Rakoto, J.M. Broto, J.C. Ousset, S. Askenazy, A.G.M. Jansen, Phys. Rev. B **49**, 3502 (1994)
8. P. Samuely, P. Szabó, T. Klein, A.G.M. Jansen, J. Marcus, C. Escribe-Filippini, P. Wyder, Europhys. Lett. **41**, 207 (1998)
9. V.F. Gantmakher, L.A. Klinkova, N.V. Barkovskii, G.E. Tsydynzhapov, S. Wiegers, A.K. Geim, Phys. Rev. B **54**, 6133 (1996)
10. D. Hall, R.G. Goodrich, C.G. Grenier, P. Kumar, M. Chaparala, M.L. Norton, Phil. Mag. B **80**, 61 (2000)
11. K. Tatsuara, N. Miura, H. Sato, S. Uchida, Physica C **212**, 459 (1993)
12. H.C. Yang, M.H. Hsieh, D.S. Lee, H.E. Horng, Phys. Rev. B **42**, 2551 (1990)
13. M.E. McHenry, M.P. Maley, G.H. Kwei, J.D. Thompson, Phys. Rev. B **39**, 7339 (1989)
14. M. Golosovsky, M. Tsindlekht, D. Davidov, Supercond. Sci. Technol. **9**, 1 (1996)
15. M.R. Trunin, Physics-Uspekhi **41**, 843 (1998)
16. J. Owliaei, S. Shridar, J. Talvacchio, Phys. Rev. Lett. **69**, 3366 (1992)
17. M.W. Coffey, J.R. Clem, Phys. Rev. B **45**, 10527 (1992)
18. E.H. Brandt, Physica C **185-189**, 270 (1991)
19. L.A. Klinkova, N.V. Barkovskii, S.A. Zver'kov, D.A. Gusev, SPCT **7**, 1437 (1994)
20. M.R. Trunin, A.A. Zhukov, A.T. Sokolov, JEPT **84**, 383 (1997)
21. A. Agliolo Gallitto, I. Ciccarello, M. Guccione, M. Li Vigni, D. Persano Adorno, Phys. Rev. B **56**, 5140 (1997)
22. T. Yokoya, A. Chainani, T. Kiss, S. Shin, K. Hirata, N. Kameda, T. Tamegai, T. Nishio, H. Uwe, Physica C **378-381**, 97 (2002)
23. S. Sahrakorpi, B. Barbiellini, R.S. Markiewicz, S. Kaprzyk, M. Lindroos, A. Bansil, Phys. Rev. B **61**, 7388 (2000)
24. J. Bardeen, M.J. Stephen, Phys. Rev. **140**, A1197 (1965)
25. J.R. Waldram, P. Theopistou, A. Porch, H.-M. Cheah, Phys. Rev. B **55**, 3222 (1997)